Journal of Materials Science: Materials in Electronics (2019) 30:10427–10434
https://doi.org/10.1007/s10854-019-01384-z

Bandgap engineered II–VI quaternary alloys and their humidity sensing performance analyzed by QCM

Sunay Turkdogan[1]

Received: 5 March 2019 / Accepted: 20 April 2019 / Published online: 26 April 2019

Abstract
In this research, growth of full composition graded II–VI materials in different morphologies using a simple but versatile chemical vapor deposition method was demonstrated and various characterizations of those materials were carried out using X-ray diffraction, scanning electron microscopy, energy dispersive spectroscopy and photoluminescence techniques. All these techniques reveal that our materials were grown in very high crystal quality and providing a unique platform to be used for many applications. In the scope of this paper, we utilized them as humidity sensing materials as they provide a wide variety of morphology change. Humidity sensing properties of those materials were investigated under various humidity levels using quartz crystal microbalance (QCM) system. It was revealed that ZnS-rich ZnCdSSe nanowires have more adsorption sites compared to the other morphologies, namely tapered nanobelt, nanosheet and thin film, and this makes them more sensitive than others. Overall, the fabricated QCM sensors exhibited fast response, high sensitivity and narrow hysteresis and therefore they are very promising for everyday appliances and various manufacturing environments with their easy operation, high sensitivity and stability, ability to work at room temperature and low cost.

1 Introduction

The use of nanostructures in various applications has been growing rapidly and attracting significant attentions due to their miniaturized size, low cost, selectivity and providing unique properties compared to their bulk counterparts [1–5]. Nanostructures with different morphologies possess high surface to volume ratio and therefore providing superior physical and chemical properties [6]. For example growing lattice-mismatched materials (up to 10%) over a single substrate is made possible by nanostructures whereas it is not possible in bulk even with 1% lattice mismatch [7–9]. On the other hand, nanostructures become more chemically reactive than bulks as the size gets smaller for the reason that majority of the atoms in the material is on its surface [6]. Unique physical properties make the structures promising especially for optoelectronic applications and the chemical properties are so crucial for gasses and humidity sensing applications.

Since sensing and controlling humidity are very crucial for everyday life appliances and a wide range of manufacturing environments such as semiconductors, food processing, pharmaceuticals, automotive and so on [10–13], it is necessary to develop a new type of humidity sensors with reliable, sensitive, and cost-effective materials and methods. A wide variety of humidity sensors based on ceramic, semiconductor, polymeric and composite materials were fabricated using different transducer methods such as capacitive [14], optical [15], acoustic [16], and impedance [17]. However, they have some drawbacks and therefore the sector is in need of new materials and sensing methods. For example, ceramic sensors are fabricated using porous semiconducting oxides, but they require a heater to recover its sensing feature [18]. Polymeric sensors on the other hand do not require a heater, but the sensor becomes less sensitive than the ceramic ones [18]. Unlike traditional humidity sensors, quartz crystal microbalance (QCM) based sensors are very promising as they offer easy operation, high sensitivity and stability, low power consumption, low cost, basic working principle and ability to work at room temperature.

Electronic supplementary material The online version of this article (https://doi.org/10.1007/s10854-019-01384-z) contains supplementary material, which is available to authorized users.

✉ Sunay Turkdogan
sunay.turkdogan@yalova.edu.tr;
sunayturkdogan@hotmail.com

[1] Department of Electrical and Electronics Engineering, Faculty of Engineering, University of Yalova, 77200 Yalova, Turkey

In the literature, there are many studies [19–32] analyzing the humidity sensing properties of various semiconductor materials using QCM method. However, to the best of our knowledge there is no any research reporting the demonstration of QCM based humidity sensors using compositionally graded II–VI materials. In this paper, we demonstrate the growth and characterization of compositionally graded II–VI materials and investigate their humidity sensing properties and the effect of morphology on that using QCM method. Furthermore, we also demonstrate how to build a complete QCM test system with a very low cost compared to the commercial counterparts.

2 Materials and methods

2.1 Growth of materials in various morphologies

Growth of materials in different morphology and composition was carried out using a custom made chemical vapor deposition (CVD) system. The schematic view and real color image of the system are shown in Fig. 1 and the system is equipped with 1-zone horizontal tube furnace (Protherm PTF 12/50/450), mullite tube, quartz tube, N_2 cylinder, rotameter, mechanical vacuum pump (Vacuubrand RZ 2.5) and various connection components. The maximum temperature of the furnace can reach up to 1200 °C, but cannot be used above 1150 °C with an extended time. The vacuum system is on the other hand fully automatic and the pressure inside the growth chamber can be set within the limits of mechanical pump (20 mTorr–760 Torr) utilizing its Pirani manometer (VSP 3000) and Vacuubrand CVC 3000 control system. It is illustrated that the reaction occurs inside the quartz tube, which is placed inside the outer mullite tube. The reason we keep the mullite tube there is not to destruct the set temperature profile of the furnace. In this research, we carried out various material growths and materials in nanostructure form were grown via vapor–liquid–solid (VLS) and vapor–solid (VS) growth methods [33, 34] while the others in thin film form were grown via VS growth method [35]. The key to grow materials in different morphology and composition within a single growth run is the temperature-dependent-composition-deposition method [36–38]. This method relies on the natural gradient of the temperature profile in the furnace.

Both precursors (CdSe and ZnS, 99.995%) were bought from Alfa Aesar and used as purchased. Si(100) and quartz wafers were used as a substrate in different growths. Substrates are mainly used as a mechanical support and construct a platform for material growth. However, substrate type with a specific thermal conductivity becomes a key factor when a growth of full composition graded materials over a single substrate is the particular interest. Before any growth initiated, temperature profile of the furnace was figured out using a long K-type external thermocouple. This was very important for the growth before reaction takes place since the heat is coming indirectly to the quartz tube by passing through the mullite tube. Because of that, the set temperature is never realized inside the quartz tube and therefore we set the furnace to 1140 °C in order to make the center of the quartz tube 1000 °C. Any given temperature along the paper will anymore refer to the real temperature at the spot (inside the quartz tube). Prior to the growth, substrates were sputtered with a thin layer of Au acting as a catalyst to initiate the nanostructure growths and then thoroughly cleaned using the typical cleaning procedures [39]. After all the preparation stages, CdSe, ZnS and substrates were placed at given positions seen in Fig. 1. Before the heating up procedure starts the growth chamber was pumped down to 30 mTorr and followed by 100 sccm (standard cubic centimeter) N_2 flow to purge oxygen inside the chamber. The carrier gas raised the system pressure up to 6 Torr. According to our experiments, the best result was gathered in 10 Torr and therefore the chamber pressure was

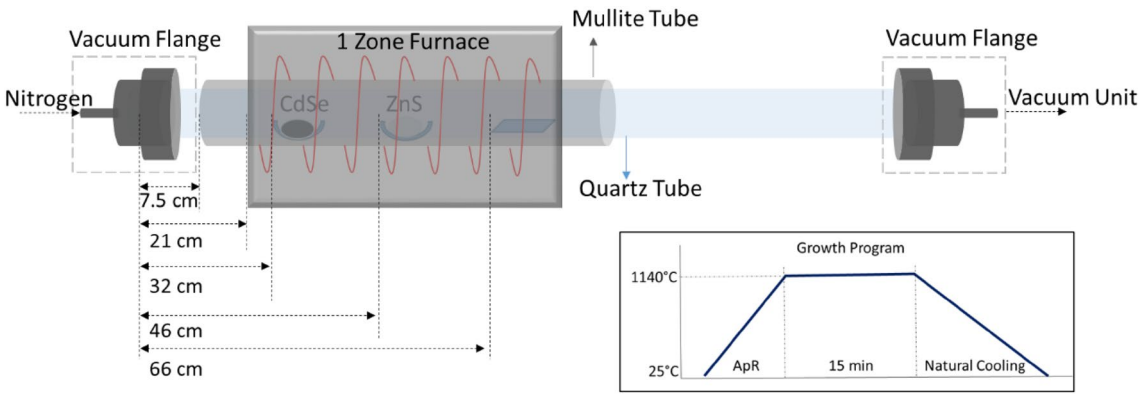

Fig. 1 Schematic view of the CVD experiment setup. Inset: growth program of a typical experiment. ApR corresponds to the heating rate of 17 °C/min

set to be 10 Torr via CVC3000 and this is done by backfilled N_2 during the growth procedure. After that, the growth program seen in Fig. 1 inset was applied and nanomaterials were grown over the substrate. During the growth procedure, 100 sccm N_2 flow was used as a carrier gas. After the growth is completed, the whole system was let to cool down naturally to the room temperature. Heating up time as denoted by ApR in Fig. 1 inset corresponds to the fastest heating up rate of the furnace (17 °C/min) and the growth was done for 15 min after the target temperature is reached. The reason the growth time is somewhat short is because of quick depletion of CdSe material due to its higher vapor pressure compared to ZnS [40]. It is important to note that in addition to nanomaterial growths we can also grow thin films using the same growth procedure excluding the Au sputtering stage. This also means that even if we aim to grow nanomaterials over the Au coated substrate we can also grow thin films over the quartz tube's surface (or quartz plate) and those can be removed easily from the surface to be utilized as a humidity-sensing medium (Fig. 2c shows such films).

2.2 Structural, chemical and optical characterizations

Morphological properties of the materials were studied using FEI QUANTA FEG 450 scanning electron microscope (SEM) at 15 kV and Olympus optical microscope. Chemical composition of the structures were figured using energy dispersive spectroscopy (EDS) detector attached to the SEM microscope. Structural properties of the materials were analyzed using PANalytical Empyrean X-ray diffractometer with Cu Kα radiation ($\lambda = 1.5406$ Å). Optical properties, specifically the band gap energies and emission characteristics of the materials were investigated using a custom made photoluminescence (PL) measurement system equipped with a HORIBA spectrometer with liquid nitrogen (LN) cooled CCD detector, 355 nm Nd:YAG pumping laser, 405 nm pumping laser diode and a fluorescent microscope (Olympus). On the other hand, humidity sensing properties of the materials were studied utilizing QCM system with 10 MHz oscillation frequency and the details will be given in the following section.

2.3 Humidity sensing of the materials using QCM technique

QCM is a widely used method to figure out the mass change on any surface as a function of the change on the quartz crystal's resonance frequency. The mass change can be calculated using Sauerbrey equation (1) for thin and uniform films [41]:

$$\Delta m = -\frac{A\sqrt{\mu\rho}}{2f_o^2}\Delta f, \tag{1}$$

where A is the active Au layer area on the crystal, μ the shear modulus of quartz, ρ density of the crystal, f_o resonance frequency of the crystal, and Δf frequency shift from its fundamental resonance frequency.

Open QCM from Novaetech Company was used to measure the resonance frequency change and the data as a function of time was recorded via USB using open QCM 1.2 software from the same company. Our QCM device utilizes an AT-cut quartz crystal with resonance frequency of 10 MHz (see Fig. 2a). AT-cut crystals are made from Y bar at 35° rotation (Fig. 2a) and widely used by the industry as it provides a stable performance over a wide temperature range (− 55 °C to 125 °C). The shear modulus (μ) and density (ρ) of the crystal are 2.947×10^{11} g/cm s^2 and 2.684 g/cm^3, respectively. According to Sauerbrey equation (1), the change of 1 Hz of the resonance frequency corresponds to − 1.255 ng of materials adsorbed on the active crystal

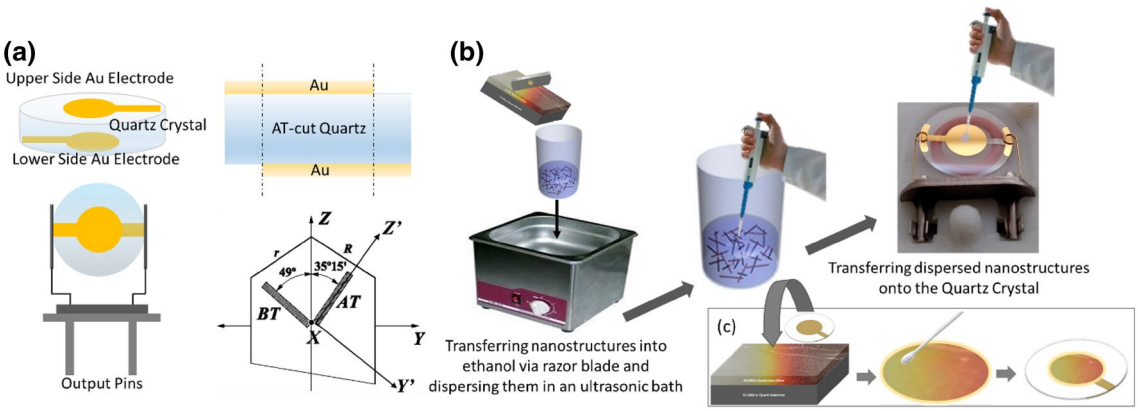

Fig. 2 **a** Sketch of the quartz crystal used in QCM based sensors. Material transfer methods to the electrode of QCM transducer. **b** Dispersion and drop cast method and **c** contact printing method

surface of 0.282735 cm^2. This number can be used interchangeably, but in case of desorption from the surface mass change becomes positive.

In order to investigate the humidity sensing properties of the materials, quartz crystal was dipped into acetone (ethanol) and sonicated in ultrasonic bath for a while and then the same crystal sonicated in DI water followed by blow dry with nitrogen. Materials were dispersed in ethanol solution using ultrasonic cleaner and then suspended materials were transferred onto the active side of the crystal by drop cast method (see Fig. 2b). The solution was dried at room temperature and in some cases evaporation of the solution was also observed from the resonance frequency shift. In addition to drop cast method to coat the crystal with materials, we also applied contact-printing method [42]. In this case, quartz crystal was flipped down over an as-grown sample to grab structures on the surface of the Au electrode. The rest also got some structures, but was cleaned using a cotton swab as illustrated in Fig. 2c.

Humidity measurements were implemented in a hermetically sealed chamber under various humidity levels. In order to adjust the moisture level inside the chamber we use two mass flow controllers (MFCs) connected to dry air cylinder as seen in Fig. 3. By changing the flow rates of those MFCs we alter the humidity level in the test chamber. As we increase the flow rate of MFC1 and MFC2 separately humidity level inside the chamber is decreased and increased, respectively. Along with QCM data we also need real humidity and temperature values inside the chamber. Therefore we designed a humidity and temperature data logger employing DHT22 sensor, SD card reader/writer and Arduino microcontroller. DHT22 sensor has sensitivity levels of ± 2–5% and ± 0.5 °C for humidity and temperature, respectively with 0.5 Hz sampling rate. It can measure humidity and temperature in the ranges of 0–100% and – 40 to 125 °C, respectively. The designed data logger is equipped with a real time clock and thus recording the humidity and temperature values as a function of time to be used to correlate the data obtained from QCM-based sensor. The details of the circuit and program embedded into the microcontroller can be found in the Supplementary Information.

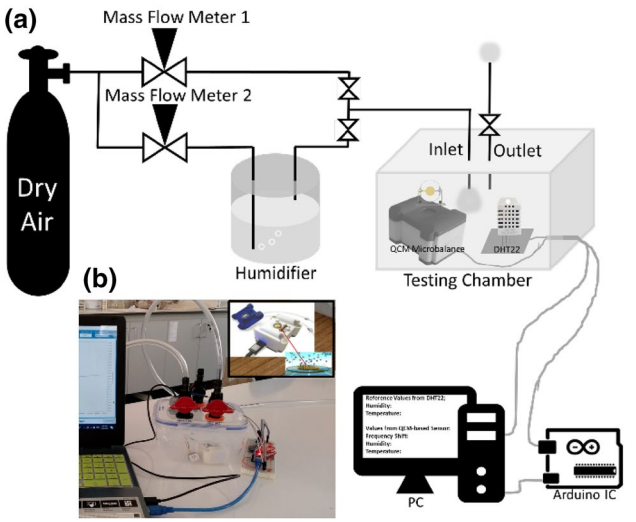

Fig. 3 **a** Schematic view of the experimental setup used to test the QCM based humidity sensors. **b** Photograph of the hermetically sealed test chamber and data logger connected to the PC. Inset: close up view of our QCM device

3 Results and discussion

3.1 Investigation of material properties

Since we utilize temperature dependent composition deposition it is important to grow full composition graded structures over a wide temperature range to understand the effect of position (or temperature) on the morphology and composition. For that purpose, we have grown many samples using various substrates as seen in Fig. 4c. It is known that the amount of material in vapor phase during the growth procedure determines the level of supersaturation and thus changing the materials morphology and chemical compositions. As mentioned above vapor pressure of ZnS is much lower than CdSe and therefore the amount of ZnS vapor always become very limited and hindering to reach a high degree of supersaturation when compared to CdSe. Therefore, it is expected to have ZnS-rich structures grown in nanowire (NW) form and CdSe-rich structures in nanosheet (NS) form. Various alloys of this material system are expected to have the morphologies between NW and NS depending on the level of supersaturation. Figure 4 shows the various characterization results from a full composition graded sample grown on a quartz substrate in a single furnace run. SEM images were taken from different spots of the sample starting from whitish color to dark brown color seen in Fig. 4c's first image. When the images checked in detail it is seen that some structures have Au tips indicating the VLS growth method. In the presence of Au catalyst, nanostructures in different morphologies can be grown depending on the supersaturation level of Au catalyst otherwise the growth results in thin film. As seen in SEM images (Fig. 4a), morphology of the materials shift from NW to NS with the length of tens of μm and width (or diameter) up to 7 μm. That means we can grow II–VI materials in any morphology just by changing the growth position (or temperature). Figure 4c is an example of different growth results where we can see the growth over a single substrate, separate substrates lying on the quartz tube or quartz plate, and thin films peeled from the growth chamber. EDS analysis was also carried out to determine the composition of materials on different spots.

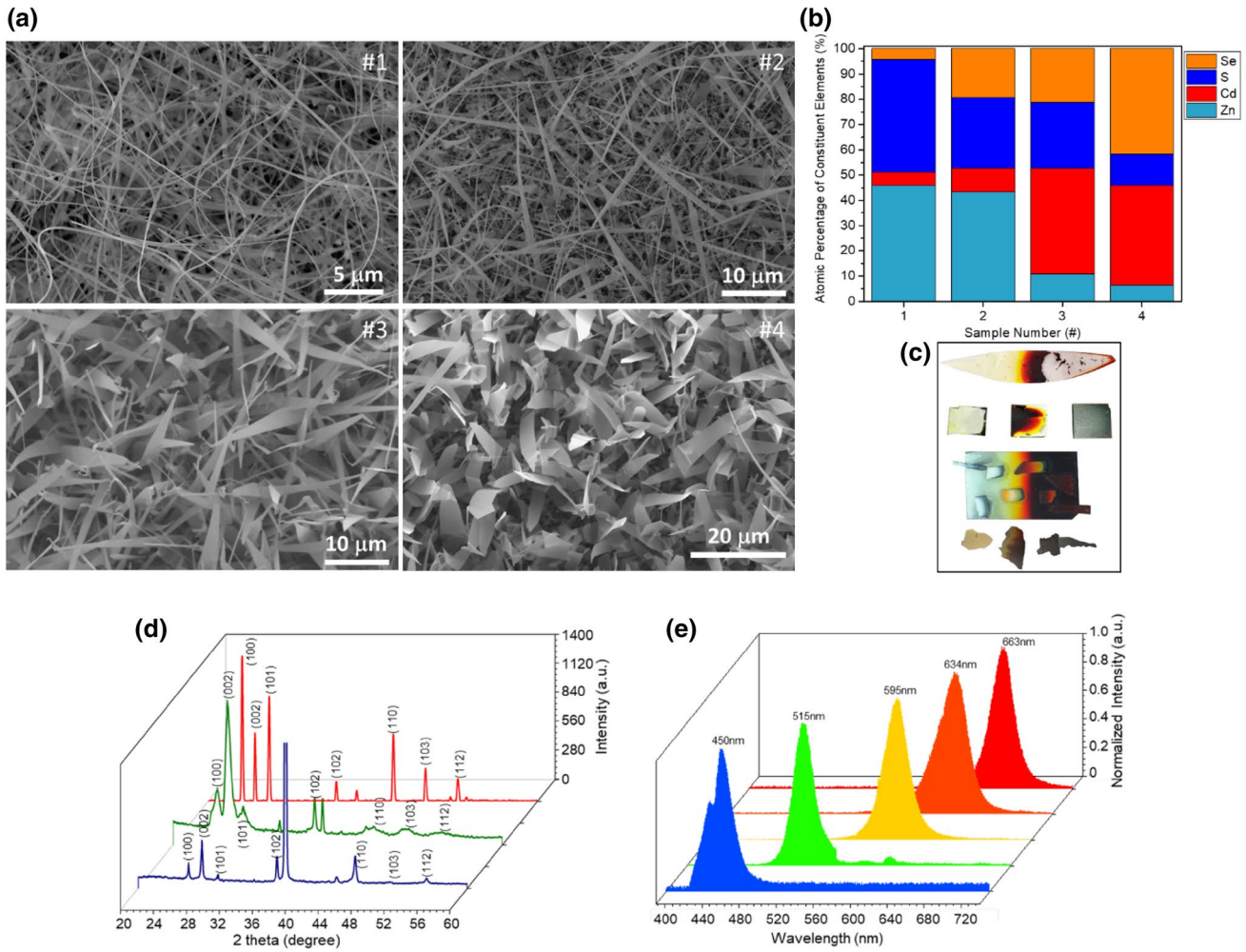

Fig. 4 **a** SEM images of quaternary alloy nanomaterials in different morphologies. **b** EDS analysis results of the sample in **a**. **c** Real color image of various samples under room light. From top to bottom, full composition graded materials over a quartz substrate, controllable composition deposition over Si substrates on quartz tube and quartz plate, and peeled thin films from the surface of quartz tube, respectively. **d** XRD and **e** PL spectra of different spots of full composition graded sample. Red shift occurs as we move from ZnS-rich ZnCdSSe to CdSe-rich ZnCdSSe materials. Spots in **b**, **d** and **e** are different and therefore composition of materials should not necessarily match (Color figure online)

As seen in Fig. 4b, materials are composed of Zn, Cd, S and Se elements and the products ended up highly stoichiometric. Sample numbers in Fig. 4b refer to the SEM images and EDS analysis results were taken from the spots seen in the SEM images. The result shows that as we move from #1 (NW-like morphology) to #4 (NS-like morphology) Cd and Se composition increase while Zn and S composition diminish.

Crystallographic properties of the same sample was figured using X-ray diffraction (XRD) and Fig. 4d shows the spectra taken from three different locations. The results reveal that alloys have wurtzite crystal structures with the characteristic peaks of (100), (002) and (101) planes between 20° and 30° of 2θ. As we move from ZnS-rich side to CdSe-rich side the characteristic peaks shift to lower degrees but the alloys stay in the region of pure CdSe (PDF Card 00-002-0330) and ZnS (PDF Card 00-001-0677). Other unmarked peaks in the higher degree region belong to SiO_2 peaks coming from the substrate. As Scherrer equation [43, 44] indicates that when the linewidth of the main peaks get narrower crystal grain size enlarges and therefore the crystal quality becomes much better. Based on that we can say that material quality gets better as we move from ZnS-rich to CdSe-rich alloy structures. Optical properties of as grown structures were studied using PL method. Figure 4e shows PL spectrums gathered from different locations over the substrate and it is clearly seen that as we move from whitish (ZnSe-rich) to blackish (CdSe-rich) side PL emission becomes red shifted as expected because bandgap energies of pure ZnS and pure CdSe are 3.91 eV and 1.74 eV corresponding to

the center emission wavelengths of 317 nm and 712 nm, respectively. PL emission spectrums centered at 450 nm, 515 nm, 595 nm, 634 nm and 663 nm were obtained from five different spots under 355 nm laser pumping and it can be imagined that we can get any color of light emission within the visible range from the ZnCdSSe quaternary alloys. All analysis results show that we can grow high quality materials using our facile and low cost growth method. Those materials can be used for various type of applications such as solar cells, photodetectors, LEDs, lasers, water splitting and etc.; however, we will utilize them as humidity-sensing materials within the scope of this work because those provide a wide morphology change. Since it determines the active adsorption sites and therefore the humidity sensing properties of the materials, a wide morphology change is an advantage for us to make a comparison between structures.

3.2 Investigation of humidity sensing properties of the materials under varying RH

Before investigating the humidity response of nanostructures it is important to mention about the humidity sensing mechanism that can be divided into two parts. First, active sites of the alloy nanostructures chemisorb water molecules [45] to link with metal ions and then more water molecules are adsorbed on the initially formed layers via Van Der Waals force [46]. In a specific humidity environment, sensors can establish an equilibrium. When the sensor is placed in a lower humidity environment, water molecules on its humidity-sensing surface will desorb resulting in a positive frequency change owing to the mass loss on the surface of QCM. Contrary to this, when the sensor is placed in a higher humidity environment, additional water molecules are adsorbed on the surface of humidity sensing materials and causes negative shift of the resonance frequency of QCM.

Figure 5a reveals the relationship of resonance frequency shift of five different sensors with relative humidity (RH) between 10 and 95%. It is obvious that deviations from the resonance frequency increase in both positive and negative ways for decreasing and increasing humidity levels, respectively. During the experiments, the humidity level of the environment was about 40% RH and at that level, it is seen that more water molecules are adsorbed on the sensor coated with NWs. As expected when the sensors placed in lower RH water molecules start to desorb from the surface and resulting positive frequency shift due to mass loss over the electrodes of quartz crystal. When it is placed at even lower RH, frequency shift increase more due to further loss of desorbed mass. As the morphology change from thin film to NW, more adsorbed molecules desorb and therefore positive frequency shift becomes more intense for NWs coated QCM than the others. Likewise, when the sensors are placed in higher RH, more water molecules are adsorbed on the surface of humidity sensing material causing the negative frequency shift. It is apparently seen in Fig. 5a that frequency shift occurs unlikely for the sensors fabricated using material in different morphology. The sensor coated with Zn-rich NWs shows greater frequency shift than the others coated with thin film, NS and nanobelt. This is as expected because as the size of the structures get smaller the specific and total surface are of the materials boost significantly and this creates a basement for more water adsorption. It is important to note that the relationship between frequency shift and RH is not linear and as the RH increases, more water molecules are adsorbed on the pre-adsorbed molecules multiplying the available adsorption sites. This phenomenon in the literature can be explained with the BET adsorption model [47]. It is noteworthy that when the sensor is over loaded QCM becomes invalid and therefore the amount of material transferred to the electrodes of AT-cut crystal should be under control and for each sensor the amount should be equal otherwise more material would cause more frequency shift with even lower RH.

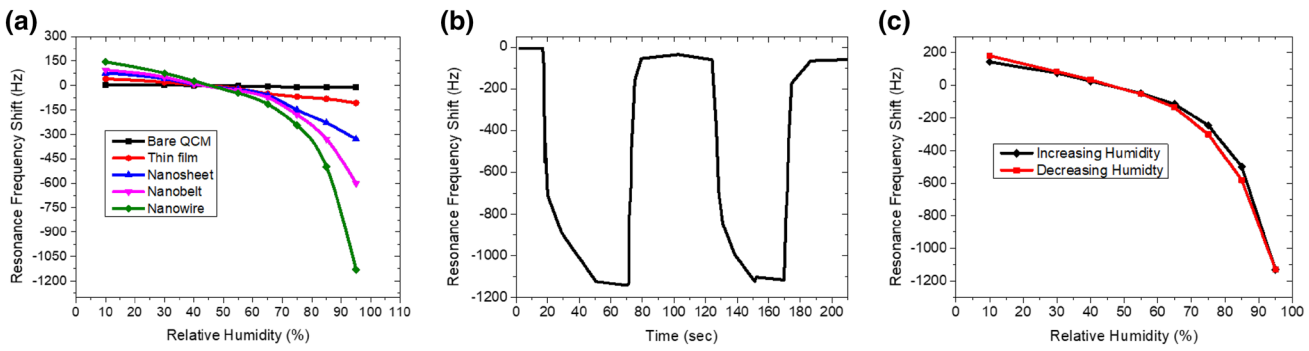

Fig. 5 **a** Frequency shift response of different sensors fabricated with materials in different morphology respect to relative humidity of the environment. **b** Repeatable sensing curve of the NWs coated QCM gathered between ~ 95% RH and ~ 40% RH. **c** Hysteresis characteristic of NWs coated QCM sensor

Response and recovery times are also very significant features of the sensors as they determine time taken to reach 90% of the frequency change for the ascending and descending humidity levels, respectively. Figure 5b shows the response curve of the sensor as a function of time under the humidity levels of 40% RH and 95% RH. Average response time of the sensor is around 21 s while the recovery time is around 8 s in average. Such rates are very promising and can be on par or even superior to the studies seen in the literature. Another factor used to evaluate the sensors' accuracy and reliability is the hysteresis indicating the time lag between descending and ascending response curves of the sensor seen in Fig. 5c. This process was conducted between ~ 10 and ~ 95% range with eight different RH values. It was found figured that the maximum hysteresis is ~ 3% under 85% RH for the best performing sensor. Since the sensor exhibits a narrow hysteresis loop under increasing and decreasing humidity, we can say that the sensor is highly accurate.

4 Conclusion

In conclusion, chemical composition and morphology tunable II–VI quaternary alloys were grown using a facile growth method employing temperature dependent composition deposition and various characterizations were carried out to figure the structural, chemical and optical properties of those materials. The results show that the materials have very high crystal quality and can be used for plenty of applications; however, in the context of this paper those were utilized as humidity sensing materials as they provide unique surface properties with varying morphologies. Humidity sensing properties of II–VI materials were investigated using a simple but very versatile QCM method and a few QCM based sensors were fabricated using materials in different morphologies to figure the effect of morphology change. Overall, QCM sensors coated with ZnS-rich ZnCdSSe NWs with their fast response (21 s response time and 8 s recovery time), high sensitivity and narrow hysteresis (3% RH) showed the best performance than others fabricated with NS, nanobelt and thin film. To the best of our knowledge, this is the first demonstration of QCM sensors based on full composition tunable ZnCdSSe quaternary alloys. In addition to optoelectronic applications, the results show that those materials are not only very promising for humidity sensing applications, but also for other gas sensing applications as the sensitivity decrease with lower surface area the sensors are less affected by water molecules and become better measurement platform to sense other harmful gasses in a humid environment.

Acknowledgements This work was supported by the Scientific Research Fund of Yalova University under the Project Number 2017/AP/140.

Compliance with ethical standards

Conflict of interests The authors declare that they have no competing interests.

References

1. E. Joanni, R. Savu, L. Valadares, M. Cilense, M.A. Zaghete, Thermal evaporation furnace with improved configuration for growing nanostructured inorganic materials. Rev. Sci. Instrum. **82**, 065101 (2011)
2. Y. Chen, C. Zhu, T. Wang, The enhanced ethanol sensing properties of multi-walled carbon nanotubes/SnO_2 core/shell nanostructures. Nanotechnology **17**, 3012–3017 (2006)
3. F.H. Ramirez, J.D. Prades, A. Hackner, T. Fisher, G. Mueller, S. Mathur, J.R. Morante, Miniaturized ionization gas sensors from single metal oxide nanowires. Nanoscale **3**, 630–634 (2011)
4. G.C. Yi, *Semiconductor Nanostructures for Optoelectronic Devices: Processing, Characterization and Applications* (Springer, Berlin, 2012)
5. S. Logothetidis, *Nanostructured Materials and Their Applications* (Springer, Berlin, 2012)
6. G. Cao, Y. Wang, Chapter 2, in *Nanostructures and Nanomaterials: Synthesis, Properties and Applications* (Imperial College Press, London, 2004)
7. T. Kuykendall, P. Ulrich, S. Aloni, P. Yang, Complete composition tunability of InGaN nanowires using a combinatorial approach. Nat. Mater. **6**, 12 (2007)
8. Y. Wang, J. Xu, P. Ren, Q. Zhang, X. Zhuang, X. Zhu, Q. Wan, H. Zhou, W. Hu, A. Pan, Bandgap broadly tunable GaZnSeAs alloy nanowires. Phys. Chem. Chem. Phys. **15**, 8 (2013)
9. S. Turkdogan, F. Fan, C.Z. Ning, Color-temperature tuning and control of trichromatic white light emission from a multisegment ZnCdSSe heterostructure nanosheet. Adv. Funct. Mater. **26**, 8521–8526 (2016)
10. S.H. Song, H.H. Yang, C.H. Han, S.D. Ko, S.H. Lee, J.B. Yoon, Metal–oxide–semiconductor field effect transistor humidity sensor using surface conductance. Appl. Phys. Lett. **100**, 101603 (2012)
11. B. Patissier, Humidity sensors for automotive, appliances and consumer applications. Sens. Actuators B **59**, 231–234 (1999)
12. D. Bridgeman, J. Corral, A. Quach, X. Xian, E. Forzani, Colorimetric humidity sensor based on liquid composite materials for the monitoring of food and pharmaceuticals. Langmuir **30**, 10785–10791 (2014)
13. D. Cartasegna, F. Conso, A. Donida, M. Grassi, L. Picolli, G. Rescio et al., Integrated microsystem with humidity, temperature and light sensors for monitoring the preservation conditions of food. Sensors **25**, 1859–1862 (2011)
14. L. Gu, Q.A. Huang, M. Qing, A novel capacitive-type humidity sensor using CMOS fabrication technology. Sens. Actuators B **99**, 491–498 (2004)
15. L. Alwis, T. Sun, K.V. Grattan, Analysis of polyimide-coated optical fiber long period grating-based relative humidity sensor. IEEE Sens. J. **13**, 767–771 (2013)
16. J.K. Kwan, J.C. Sit, High sensitivity Love-wave humidity sensors using glancing angle deposited thin films. Sens. Actuators B **173**, 164–168 (2012)

17. H.T. Hsueh, S.J. Chang, F.Y. Hung, C.L. Hsu, B.T. Dai, K.T. Lam, K.H. Wen, A flexible ZnO nanowire-based humidity sensor. IEEE Trans. Nanotechnol. **11**, 520–525 (2012)
18. B.M. Kulwicki, Humidity sensors. J. Am. Ceram. Soc. **74**, 697–708 (1991)
19. V.P. Anju, P.R. Jithesh, S.K. Narayanankutty, A novel humidity and ammonia sensor based on nanofibers/polyaniline/polyvinyl alcohol. Sens. Actuators A **285**, 35–44 (2019)
20. Y.N. Guo, Z.Y. Gao, X.X. Wang, L. Sun, X. Yan, S.Y. Yan, W.P. Han, A highly stretchable humidity sensor based on spandex covered yarns and nanostructured polyaniline. RSC Adv. **8**, 1078–1082 (2018)
21. K.N. Chappanda, O. Shekhah, O. Yassine, S.P. Patole, M. Eddaoudi, K.N. Salama, The quest for highly sensitive QCM humidity sensors: the coating of CNT/MOF composite sensing films as case study. Sens. Actuators B **257**, 609–619 (2018)
22. X. Cha, F. Yu, Y. Fan, J. Chen, L. Wang, Q. Xiang, J. Xu, Superhydrophilic ZnO nanoneedle array: controllable in situ growth on QCM transducer and enhanced humidity sensing properties and mechanism. Sens. Actuators B **263**, 436–444 (2018)
23. T.A. Blank, L.P. Eksperiandova, K.N. Belikov, Recent trends of ceramic humidity sensors development: a review. Sens. Actuators B **228**, 416–442 (2016)
24. X. Chen, X. Chen, N. Li, X. Ding, X. Zhao, A QCM humidity sensors based on GO/Nafion composite films with enhanced sensitivity. IEEE Sens. J. **16**, 8874–8883 (2016)
25. Y. Yao, X. Chen, W. Ma, W. Ling, Quartz crystal microbalance humidity sensors based on nanodiamond sensing films. IEEE Trans. Nanotechnol. **13**, 386–393 (2014)
26. N. Asar, A. Erol, S. Okur, M.C. Arikan, Morphology-dependent humidity adsorption kinetics of ZnO nanostructures. Sens. Actuators A **187**, 37–42 (2012)
27. S. Okur, N. Üzar, N. Tekgüzel, A. Erol, M.Ç. Arıkan, Synthesis and humidity sensing analysis of ZnS nanowires. Physica E **44**, 1103–1107 (2012)
28. A. Erol, S. Okur, N. Yağmurcukardeş, M.Ç. Arıkan, Humidity-sensing properties of a ZnO nanowire film as measured with a QCM. Sens. Actuators B **152**, 115–120 (2011)
29. A. Erol, S. Okur, B. Comba, Ö. Mermer, M.C. Arıkan, Humidity sensing properties of ZnO nanoparticles synthesized by sol–gel process. Sens. Actuators B **145**, 174–180 (2010)
30. F. Pascal-Delannoy, B. Sorli, A. Boyer, Quartz crystal microbalance (QCM) used as humidity sensor. Sens. Actuators A **84**, 285–291 (2000)
31. K. Galatsis, W. Qu, W. Wlodarski, Quartz crystal microbalance humidity sensor with porous electrodes, in *1998 Conference on Optoelectronic and Microelectronic Materials Devices, 1998. Proceedings* (IEEE, 1999), pp. 373–375
32. Ş.D. Zor, H. Cankurtaran, QCM humidity sensors based on organic/inorganic nanocomposites of water soluble-conductive poly (diphenylamine sulfonic acid). Int. J. Electrochem. Sci. **11**, 7976–7989 (2016)
33. R.S. Wagner, W.C. Ellis, Vapor–solid–liquid mechanism of single crystal growth. Appl. Phys. Lett. **4**, 89 (1964)
34. F. Fan, S. Turkdogan, Z. Liu, D. Shelhammer, C.Z. Ning, A monolithic white laser. Nat. Nanotechnol. **10**, 796 (2015)
35. G.H. Gilmer, G.H. Marcia, Models of thin film growth modes. JOM **39**, 6 (1987)
36. Y. Liu, J.A. Zapien, Y.Y. Shan, C.Y. Geng, C.S. Lee, S.T. Lee, Wavelength controlled lasing in $Zn_xCd_{1-x}S$ single crystal nanoribbons. Adv. Mater. **17**, 1372–1377 (2005)
37. Y. Liu, J.A. Zapien, Y.Y. Shan, H. Tang, C.S. Lee, S.T. Lee, Wavelength-tunable lasing in single-crystal $CdS_{1-x}Se_x$ nanoribbons. Nanotechnology (2007). https://doi.org/10.1088/0957-4484/18/36/365606
38. J.A. Zapien, Y. Liu, Y.Y. Shan, H. Tang, C.S. Lee, S.T. Lee, Continuous near-infrared-to-ultraviolet lasing from II–VI nanoribbons. Appl. Phys. Lett. **90**, 213114 (2007)
39. S. Turkdogan, Growth and Characterization of Multisegment Chalcogenide Alloy Nanostructures for Photonic Applications in a Wide Spectral Range, Dissertation, Arizona State University, 2015
40. *Thin Film Evaporation Guide* (Lebow Corporation and Vacuum Engineering and Materials, Inc., Santa Clara, 2008)
41. G. Sauerbrey, The use of quartz crystal oscillators for weighing thin layers and for microweighing applications. Z. Phys. **155**(3), 206–222 (1959)
42. T. Takahashi, P. Nichols, K. Takei, A.C. Ford, A. Jamshidi, M.C. Wu, C.Z. Ning, A. Javey, contact printing of compositionally graded CdS_xSe_{1-x} nanowire parallel arrays for tunable photodetectors. Nanotechnology (2012). https://doi.org/10.1088/0957-4484/23/4/045201
43. A.L. Patterson, The Scherrer formula for X-ray particle size determination. Phys. Rev. **56**, 10 (1939)
44. A. Monshi, M.R. Foroughi, M.R. Monshi, Modified Scherrer equation to estimate more accurately nano-crystallite size using XRD. WJNSE **2**, 154 (2012)
45. M. Su, J. Wang, Y. Hao, Development of Y^{3+} and Mg^{2+}-doped zirconia thick film humidity sensors. Mater. Chem. Phys. **126**, 31–35 (2011)
46. L. Gu, K. Zheng, Y. Zhou, J. Li, X. Mo, G.R. Patzke, G. Chen, Humidity sensors based on ZnO/TiO_2 core/shell nanorod arrays with enhanced sensitivity. Sens. Actuators B **159**, 1–7 (2011)
47. X. Zhou, J. Zhang, T. Jiang, X. Wang, Z. Zhu, Humidity detection by nanostructured ZnO: a wireless quartz crystal microbalance investigation. Sens. Actuators A **135**, 209–214 (2007)